Available online at www.sciencedirect.com
SCIENCE DIRECT®
Sensors and Actuators A 117 (2005) 241–251
SENSORS AND ACTUATORS A PHYSICAL
www.elsevier.com/locate/sna

# A new method for membrane-based gas measurements

D. Lazik*, H. Geistlinger

*Department of Hydrogeology, UFZ Centre for Environmental Research Leipzig-Halle, T.-Lieser-Strasse 4, 06120 Halle, Germany*

Received 16 February 2004; received in revised form 7 June 2004; accepted 10 June 2004
Available online 27 July 2004

**Abstract**

A method for gas measurement based on selective diffusion of gases through membrane tubes has been developed. Combining the element-specific diffusion rates through a membrane set and Dalton's principle of partial pressures, the gas concentration is determined through measured physical quantities: pressure, time, and temperature. Since the procedure is based on the evaluation of an intensive thermodynamic state variable, miniaturization of the sensor is possible. The gas sensor consists of several measuring chambers closed by membranes, where each chamber has its own pressure sensor. One additional sensor is used for temperature measurement. The measurement is carried out after the conditioning of the measuring chambers with a purge gas, which is used as internal standard. In order to determine the *m* partial pressures of the components by *n* pressure measurements, a system of linear equations has to be solved. The measuring method is demonstrated for a two-component-gas phase (oxygen, nitrogen) for a partial pressure range from 0.1 to 100 kPa. The mean absolute error of about 5% related to the measurement value is acceptable and can be reduced further, if the technical deficiencies of the experimental set-up are improved.


*Keywords:* Gas measurement; Membrane; Permselectivity

## 1. Introduction

Membranes, particularly those based on polymers, gain increasing importance for gas measurement. First, membranes are used as a *gas-permeable phase boundary*, e.g. between a water and a gas phase, i.e. as a window between test object and measuring device, that can be passed only by gases. This application of phase separating membranes is used since decades by applied sciences, medicine, and industry for gas analysis: (a) environmental gas analyses with lab gas chromatographs are based on the equilibration of the gas composition of the relevant environmental compartment with the interior of closed polymer bottles, (b) membrane-based catheters for in vivo-analysis of blood gas composition [1], (c) membrane-based measurements for process control in the food industry, e.g. the adjustment of $CO_2$ concentration during beverage manufacture [2], or (d) solid-state gas sensors are encapsulated with gas-permeable membrane films [3].

On the other hand, the *gas-selective properties* of membranes are increasingly used for direct gas analysis. Recent efforts focus on the investigation and utilization of the gas-dependent electrical conductivity [4], the gas-dependent swelling behavior [5] and, the gas-dependent colour reactions (e.g. in [6]).

For the estimation of the absolute gas pressure Weiss [7] develops a gas saturometer: the dissolved gas concentration in a liquid is measured behind a phase-separating silicone membrane at equilibrium. In case that only a pure gas (one component) is dissolved in the liquid the saturometer gives the concentration of the gas by applying Henry's law. This principle is adapted since 1983, e.g. for estimating and controlling the $CO_2$ concentration of beer [8]. Six years later a flux-based method [9] was developed in order to overcome the relatively large equilibration times of the $CO_2$-partial pressure. For the estimation of the partial pressures of further gas components alternative methods are still in use.

In order to find a component-independent gas measurement method we consider the gas-selective properties of membranes. The developed method is based on the

* Corresponding author. Tel.: +49 345 558 5209; fax: +49 345 558 5559.
*E-mail address:* detlef.lazik@ufz.de (D. Lazik).

0924-4247/$ – see front matter © 2004 Elsevier B.V. All rights reserved.
doi:10.1016/j.sna.2004.06.015

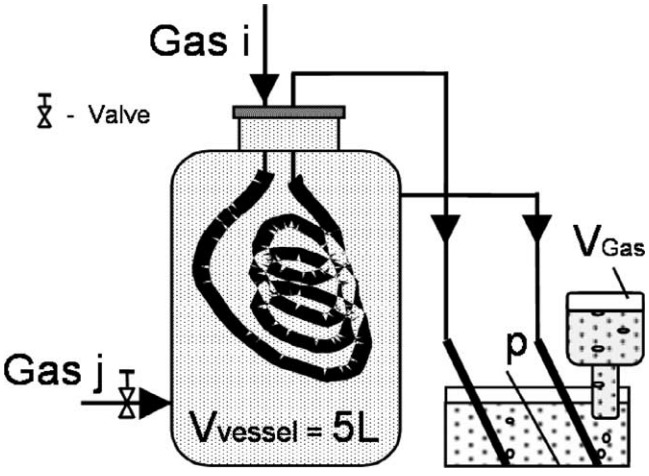


Fig. 1. Experiment illustrating the gas sensor working principle.

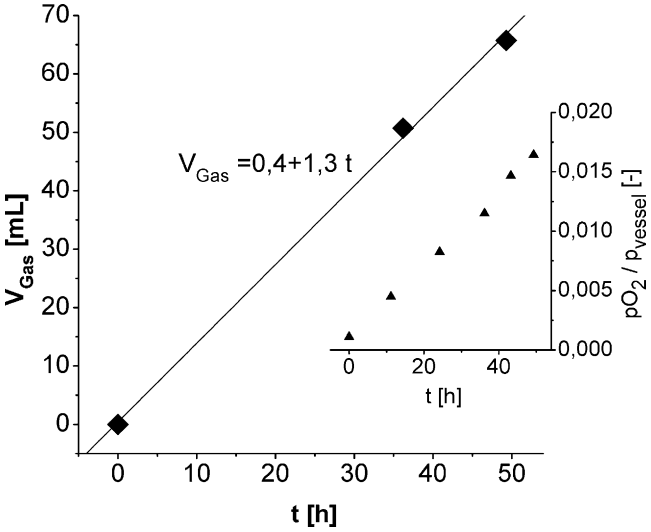


Fig. 2. The linear time dependence of the trapped gas volume $V_{gas}$ (squares) and $O_2$ concentration in the 5 L vessel (triangles).

proportions in the permeation rates (permselectivity) of gases through membranes, whereby a common internal standard is used [10].

The measuring principle is explained by the following instructive experiment:

A gas-selective PTFE-membrane tube (length $L$ = 8.57 m, inner and outer radius $R_i$ = 0.5 mm, $R_a$ = 1.5 mm) is located in a relatively large closed vessel. Through this membrane tube oxygen (gas i) flows and discharges in a water-filled container (left output) (see Fig. 1).

The vessel is simultaneously flushed with nitrogen (gas j), which likewise discharges in the water container from the right output. Therefore, the partial pressures of both gases are equal and correspond to the gas pressure that is necessary to compensate the hydrostatic pressure at the bottom of water container. Oxygen (gas i) will diffuse through the membrane into the container due to the concentration gradient, whereas nitrogen (gas j) will diffuse into the tube interior, because of the opposite gradient. After diffusive fluxes have reached the stationary state, the nitrogen supply is interrupted.

Because of the large vessel volume the nitrogen partial pressure remains nearly constant for the next hours, i.e. the oxygen flux is driven by a nearly constant gradient. Then a water-filled bottle (receptacle) is placed above the emerging nitrogen gas bubbles. These bubbles are collected with the receptacle and represent the volume increase for the two-component-gas system (see Fig. 2).

The ordinate on the right of Fig. 2 represents the $O_2$ concentration measured in the 5 L vessel. Due to the high dilution volume, the oxygen partial pressure remains low during the whole experiment and can be neglected. Therefore, the individual gas concentrations on either membrane side remain almost constant during the test: pure oxygen gas inward the tube and pure nitrogen outward the tube. The observed volume increase is caused by the different permeation fluxes of the two gas components—oxygen and nitrogen, i.e. by the permeation-selective (permselective) property of the membrane.

The combination of different membranes for a multi-component gas system is the bases of our new measuring method; its theoretical basics are derived in the following section.

## 2. Theoretical basics

There are two physical pictures in the literature for the permeation process of gases through membranes (a) for porous membranes the gas flows through pore channels (Hagen–Poiseuille-law) and (b) for dense membranes the gas migrates via diffusion. All subsequent derivations are based on the diffusion picture (b), i.e. the assumption that the solution–diffusion model is applicable and that the diffusion properties of the near-surface layer and the interior of the membrane do not differ (dense symmetrical membrane).

According to the solution–diffusion model, permeation proceeds in several steps. In the first step, gas is adsorbed from adjacent space at the outer membrane surface ($R_a$, Fig. 3).

Once the gas molecule is adsorbed, desorption or absorption will occur depending on the energetics of the surface. Absorption, which is considered as dissolution process (gas molecules are dissolved into the membrane phase), is the rate limiting step, compared to the fast adsorption process. Inside the membrane the gas molecules diffuse according to the concentration gradient along the membrane radius. If the gas molecules reach the inner membrane surface at $R_i$, the mass transfer proceeds in reverse order: gas leaves the membrane phase and is subsequently desorbed into the gas phase.

### 2.1. Single-component system

Since both the adsorption–desorption processes and the gas phase diffusion process are fast processes compared to

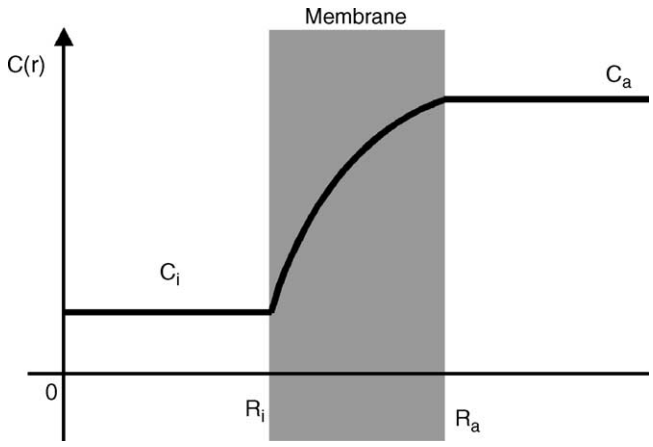


Fig. 3. Schematic representation of the stationary concentration profile $C(r)$ in a tubular polymer membrane for given concentrations in the external ($C_a$) and the internal ($C_i$) space.

the diffusion process within the solid membrane phase, an adsorption–desorption equilibrium and constant concentrations in both adjacent gas spaces can be assumed.

At sufficiently low concentrations, the in general non-linear adsorption isotherm can be approximated by a linear Henry isotherm

$$\frac{p_k^{\mathrm{a}}}{RT} = C_k^{\mathrm{a}} = H_k^{\mathrm{a}} C_k(r = R_{\mathrm{a}}), \tag{1}$$

where $p_k^{\mathrm{a}}$ [Pa] denotes the partial pressure of component $k$ in the external space, $C_k^{\mathrm{a}}$ [mol/L] the corresponding gas concentration according to the ideal gas law, and $C_k(r)$ [mol/L] the concentration in the membrane phase ($R = 8.31447$ J/(K mol), gas constant; $T$ [K], temperature; $r$ [m], radius).

The dimensionless Henry constant $H_k^{\mathrm{a}}$ describes the solution equilibrium. The inverse Henry constant is referred to as solubility $S_k^{\mathrm{a}}$:

$$C_k(r = R_{\mathrm{a}}) = S_k^{\mathrm{a}} C_k^{\mathrm{a}} \tag{2}$$

The corresponding boundary condition for the interior space is given by ($p_k^i$ [Pa], $C_k^i$ [mol/L]—partial pressure and concentration of component $k$ in interior space, respectively):

$$C_k(r = R_i) = S_k^i C_k^i = \frac{C_k^i}{H_k^i} = \frac{p_k^i}{RTH_k^i}. \tag{3}$$

For a symmetrical membrane (index '$M$') in a gaseous phase (index '$G$') holds:

$$H_k^i = H_k^{\mathrm{a}} \equiv H_k^{MG} = \frac{1}{S_k^{MG}}, \quad (H^{M,G}[m_M^3/m_G^3]) \tag{4}$$

The flux density $j_k(r, t)$ [mol/(m$^2$ s)] through a membrane is described by Fick's First Law:

$$j_k(r, t) = -D_k \frac{\partial C_k(r, t)}{\partial r} \tag{5}$$

($D_k$ [m$^2$/s]—diffusion coefficient of gas component $k$ in the membrane). Assuming that both the solubility and the diffusion coefficient are concentration independent, the stationary flow $Q$ [mol/s] through the membrane can be calculated analytically:

$$\begin{aligned} Q_k &= \frac{\mathrm{d}\nu_k}{\mathrm{d}t} = j_k(r) 2\pi r L = S_k D_k \frac{(p_k^{\mathrm{a}} - p_k^i)}{RT} \frac{2\pi L}{\ln(R_{\mathrm{a}}/R_i)} \\ &= \text{const}, \\ r &= \{R_i, R_{\mathrm{a}}\}, \end{aligned} \tag{6}$$

($\nu_k$—amount of substance). As a result, the entire migration process is determined by the product of two material parameters, solubility and diffusion coefficient. This product is called in the literature permeability $P_k$ [m$^2$/s]:

$$P_k = S_k D_k. \tag{7}$$

Eq. (8) gives the number of moles $\mathrm{d}\nu_k$ that permeate in a certain time $\mathrm{d}t$ through the membrane into the interior space:

$$\mathrm{d}\nu_k = P_k \frac{p_k^{\mathrm{a}} - p_k^i}{RT} \frac{2\pi L}{\ln(R_{\mathrm{a}}/R_i)} \mathrm{d}t \tag{8}$$

One can substitute the mol number in Eq. (8) using the ideal gas law:

$$V_0(p_0 + \mathrm{d}p_k) = p_0(V_0 + \mathrm{d}V_k) = RT(\nu_0 + \mathrm{d}\nu_k) \tag{9}$$

where $V_0$ [m$^3$] is volume, $p_0$ [Pa] the pressure, $\nu_0$ [mol] the number of moles inside the measuring chamber, lower index '0' indicates the initial state.

It obtains the following expression for the volume change under isobaric conditions:

$$\mathrm{d}V_k = \frac{RT}{p_0} \mathrm{d}\nu_k = P_k \frac{p_k^{\mathrm{a}} - p_k^i}{p_0} \frac{2\pi L}{\ln(R_{\mathrm{a}}/R_i)} \mathrm{d}t, \tag{10}$$

and for the equivalent pressure change isochoric conditions (e.g. a closed tubular membrane), respectively:

$$\mathrm{d}p_k = \frac{RT}{V_0} \mathrm{d}\nu_k = P_k \frac{p_k^{\mathrm{a}} - p_k^i}{V_0} \frac{2\pi L}{\ln(R_{\mathrm{a}}/R_i)} \mathrm{d}t \tag{11}$$

For a stationary isobaric process Eq. (10) can be integrated over time, leading to a linear volume increase with time (compare with the observed volume increase in Fig. 2).

### 2.2. Multi-component system

For a multi-component system—superposition of the different migrating gas components is assumed as a first approximation. According to Dalton's law the total pressure on both sides of the membrane is given by the sum of the partial pressures:

$$p^{\mathrm{a},i} = \sum_{k=1}^{n} p^{\mathrm{a},i} \tag{12}$$

and the pressure change inside the tube is

$$\mathrm{d}p = \sum_{k=1}^{n} \mathrm{d}p_k = g \sum_{k=1}^{n} P_k (p_k^{\mathrm{a}} - p_k^i)\,\mathrm{d}t, \tag{13a}$$

where the pressure changes of $n$ gas components are described by Eq. (11) and a geometry factor $g$ [1/m$^2$] of the measuring chamber has been introduced:

$$g = \frac{1}{V_0} \frac{2\pi L}{\ln(R_{\mathrm{a}}/R_i)}. \tag{13b}$$

Let us assume that at time $t = 0$ (start of measurement) the measuring chamber contains only the purging gas ($k = s$)

$$\sum_{k=1}^{n} p^i = p_s^i(t=0) = p_0 \tag{14a}$$

and the partial pressures outside the tube are constant during the measuring run

$$p_k^a = \text{const.} \tag{14b}$$

Using this, Eq. (13a) can be simplified and one obtains

$$\left.\frac{\mathrm{d}p(t)}{\mathrm{d}t}\right|_{t=0} = g P_s \left[\sum_{k=1}^{n} f_{ks} p_k^{\mathrm{a}} - p_0\right], \tag{15a}$$

where the dimensionless permselectivity coefficients $f_{ks}$ were defined with regard to the purging gas:

$$f_{ks} = \frac{P_k}{P_s}. \tag{15b}$$

Since the gas analysis is based on the evaluation of Eq. (15a), one needs the pressure change for the initial time ($t = 0$; start of measurement). The main problem is that a priori this value is not known and has to be determined by extrapolation:

Recording the time-dependent pressure values $p_i = p(t_i)$ at subsequent times $t_i$ for $t > 0$, one can approximate the discrete pressure values using the polynomial:

$$F(t) = \sum_{p} a_p t^p \text{ [Pa]}, \tag{16a}$$

In order to achieve the best fit, one has to minimize the following objective function:

$$\sum_{i} (p(t_i) - F(t = t_i))^2 = \text{Min.} \tag{16b}$$

For $t \to 0$, the approximated pressure change is determined only by the coefficient $a_1$:

$$\lim_{t\to 0} \frac{\mathrm{d}F(t)}{\mathrm{d}t} = a_1. \tag{17}$$

Using the analytical solution for a very thin membrane (for derivation see Appendix A):

$$p_k^i(t) = p_k^{\mathrm{a}} + (\,p_k^i\big|_{t=0} - p_k^{\mathrm{a}}) \exp(-\kappa_k t), \tag{18}$$

and Dalton's law for the total pressure:

$$p(t) = \sum_{k=1}^{n} p_k^i(t), \tag{19}$$

a Taylor expansion of Eq. (18) for small times dt yields an analytical expression for d$p(t)$:

$$p(t) = p_0 + \mathrm{d}p(t) = \sum_{k=1}^{n} \left\{\, p_k^i\big|_{t=0} (1 - \kappa_k\,\mathrm{d}t) + p_k^{\mathrm{a}} \kappa_k\,\mathrm{d}t \right\}, \tag{20}$$

where $\kappa_k = gP_k$ [s$^{-1}$]. In order to prove that the steady-state solution yields the exact limit, one has to insert the initial condition Eq. (14) into Eq. (20), which leads again to Eq. (15).

Equating Eq. (15a) with Eq. (17) gives the basic equation for the measurement evaluation:

$$\sum_{k=1}^{n} f_{ks} p_k^{\mathrm{a}} = p_0 + \frac{a_1}{g P_s}; \tag{21}$$

i.e. the unknown partial pressures $p_k^{\mathrm{a}}$ are now functions of the coefficient $a_1$, which is determined by the experimental pressure increase.

Using $m$ membranes of different permselectivities $f_{ns}^m$ for the measurement, the $m$ describing equations form a system of linear algebraic equations:

$$\begin{pmatrix} f_{1s}^1 & f_{2s}^1 & \cdots & f_{ns}^1 \\ f_{1s}^2 & \cdots & \cdots & \cdots \\ \cdots & \cdots & \cdots & \cdots \\ f_{1s}^m & \cdots & \cdots & f_{ns}^m \end{pmatrix} \begin{pmatrix} p_1^a \\ p_2^a \\ \cdots \\ p_n^a \end{pmatrix} = \begin{pmatrix} p_0^1 + \dfrac{a_1^1}{g^1 P_s^1} \\ p_0^2 + \dfrac{a_1^2}{g^2 P_s^2} \\ \cdots \\ p_0^m + \dfrac{a_1^m}{g^m P_s^m} \end{pmatrix}, \quad m \geq n. \tag{22}$$

Its solution determines the $n$ unknown partial pressures $p_k^{\mathrm{a}}$.

The factors $g^i$ in Eq. (22) take into account the geometry of the measuring chambers.

### 2.3. Test criterion

The sum of the partial pressures (total gas pressure) of the multi-component gas phase is denoted by $p^{\mathrm{equ}}$ and can be measured simultaneously and independently. The application of Dalton's principle to the solution vector Eq. (22) gives a performance and balance criterion $G$ for the cautious evaluation of the measuring error:

$$G = \frac{1}{p^{\mathrm{equ}}} \sum_{j} p_{\mathrm{a}}^j - 1, \tag{23}$$

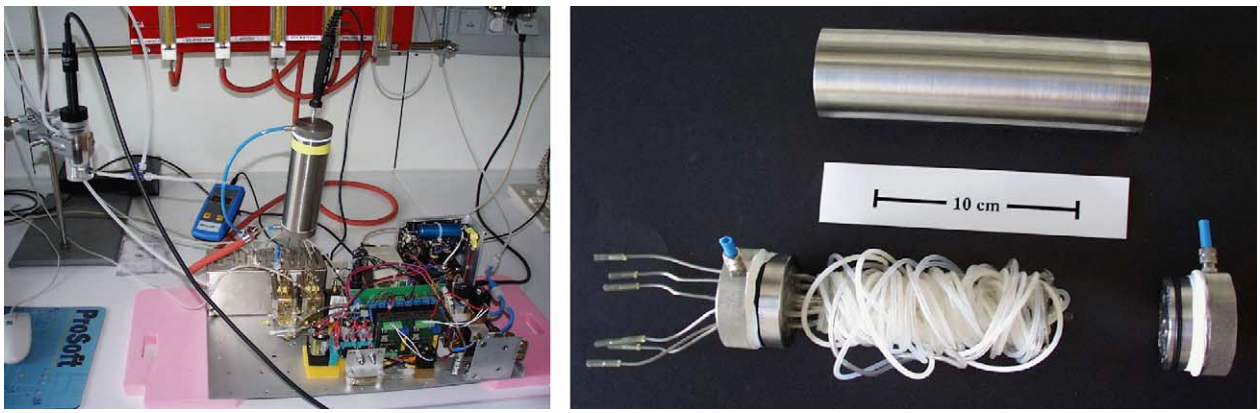


Fig. 4. Gas sensor: prototype (left) and test vessel (right).

## 3. Experiments

### 3.1. Sensor

The sensor consists of several membrane-covered measuring chambers, where each of these contains a pressure sensor. Two valves per chamber allow purge-gas flushing—for example with nitrogen.

Figs. 4 and 5 show the gas sensor prototype and the experimental set-up.

The membranes (in this study: polymer tubes, see Fig. 4 right) are located inside of a test vessel, so that the external tube surfaces are in contact with the gas to be analyzed. The test vessel consists of a stainless-steel cylinder with a screw-on cover, which has six capillary tube connections (inserted capillary tubes: $L$ = 10 cm, $R_i$ = 0.5 mm) plus two additional tube connections for flushing with the gas mixtures of interest. Three commercially available polymer tubes (Table 1) were connected with the capillary tubes and wound round a rod passing axially through. Then the membrane tube-equipped test vessel was closed.

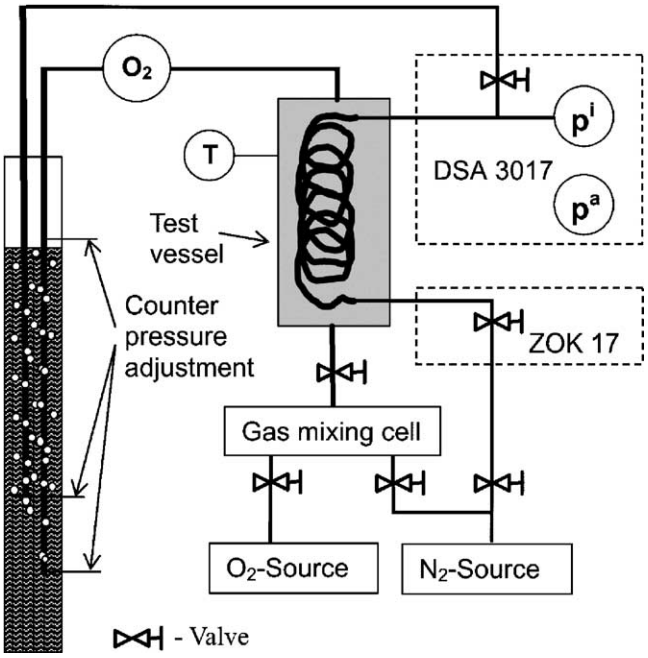


Fig. 5. Experimental setup (illustrated for one measuring chamber).

The capillary tubes were connected to the pressure scanner DSA 3017[1] and the valve block ZOK17[2] so that every membrane tube, mounted between one valve of each component, forms a lockable measuring chamber (Fig. 5).

About 90% of the internal volume $V_0$ of the measuring chambers assembled in this way is determined by the tube internal volume interfacing with the membrane. The additional dead volume located between the valves in ZOK 17 and DSA 3017 (Fig. 5) was about 160 mm$^3$ for each measuring chamber $m$ and is implicitly considered in the geometry factor $g^m$.

Further pressure sensors serve for the measurement of air pressure[3] and the pressure inside the test vessel $p^a$. In order to record the temperature a Pt 1000-sensor was attached to the test vessel. Experiments and data acquisition were controlled by PC support.

### 3.2. Experimental set-up and gas analysis procedure

The sample gas mixtures with constant component ratios are adjusted in a gas mixing cell through two pressure reducing valves (see Fig. 5) using the laboratory gas supply.

The mixing cell was equipped with an outlet valve for dosing the gas flow. The gas mixture was flushed through both the test vessel and a reference $O_2$ sensor, where the gas flows

[1] Scanivalve Corp., full range scales for $p^i$: ±35 kPa, and for $p^a$: 105 kPa, difference pressure with respect to the air pressure with common reference, accuracy ± 0.05%fs.

[2] Valve block, which is also used with the same structure in DSA 3017. Scanivalve Corp.

[3] HPB, Honeywell Corp., full range scale 50–120 kPa absolute pressure, accuracy ± 0.03%fs.

Table 1
Characteristics of membranes and measuring chambers

| Measuring chambers | Membrane tube | $R_i$ (mm) | $R_a$ (mm) | $L$ (mm) | $g^m$ (1/mm$^2$) |
|---|---|---|---|---|---|
| S1 | Silicone | 0.4 | 1.2 | 4082 | 10.55 |
| S2 | Tygon no. 3603 | 0.4 | 1.2 | 4019 | 10.54 |
| S3 | C-Flex | 0.4 | 1.2 | 4020 | 10.54 |

were determined by the adjustment of gas counterpressures (0–35 kPa water column + air pressure).

Reference $O_2$[4] — and test vessel pressure sensors are used for the independent analysis of $N_2/O_2$ mixtures with respect to:

$$p^a = p_{O_2} + p_{N_2}. \quad (24)$$

An analysis consists of the two steps: (1) membrane conditioning and, (2) measurement of the time-dependent chamber pressures.

### 3.2.1. Step 1: membrane conditioning

The test vessel is flushed with the unknown gas mixture, whereas the measuring chambers, i.e. our lockable membrane tubes, are flushed with nitrogen. In order to avoid elastical deformations of the membranes, the pressures inside the measuring chambers were fixed in correspondence to the test vessel pressure by adjustment of the counterpressure (see Fig. 5).

After the relaxation time $\tau_C$ [s] the steady-state flux is achieved and the conditioning step is finished. This relaxation or conditioning time depends on the membrane thickness, on its permeability, and on the required precision of the gas analysis, too. It can be estimated with respect to the lowest permeability $P_{min}$ of the gases of interest by:

$$\tau_C = \frac{\xi}{P_{min}}(R_a - R_i)^2, \quad (25)$$

where the number $\xi$ defines the deviation of the non-steady flux from the steady-state ones. The solution of the corresponding instationary diffusion equation yields for $\xi = 2$ an approximation of 99% of the stationary flux respectively, for $\xi = 2.5$ one obtains 99.7%, and so far.

### 3.2.2. Step 2: measurement

The measurement starts by closing the purging gas flow valves. Pressures on both sides of the membranes, time, and temperature are recorded. The measurement stops either after the pre-set measuring time has expired or if the measuring range of the pressure sensor is exceeded. In the latter case gas flow valves are opened.

[4] Oxi 330 with galvanic measuring chamber CellOx 225, WTW Corp., full range scale $p_{O_2} < 100$ kPa, accuracy: 1% of measurement value (with sufficient flow), steadying time $t_{99} < 60$ s. The electrolyte-filled $O_2$ sensor is intended by the manufacturer to be used for measurement in aqueous solutions. To prevent the electrolyte from drying up, it was always dismounted after measurements.

### 3.3. Experimental realization

Before each experiment the slope of the oxygen reference sensor was calibrated against air. The reference measuring values were recalculated into the $p^a$—dependent $O_2$ partial pressures using previously performed measurements against the test vessel filled with pure oxygen and the corresponding absolute pressure $p^a$.

The $N_2$ partial pressure inside the test vessel was estimated as difference to the $O_2$ partial pressure according to Eq. (24) using the measured pressure $p^a$.

Eq. (25) was used as the basis for estimating the time for Step 1—conditioning of membranes with $\xi \geq 2$. The Measurements (Step 2) were carried out over a time period of about 200 s and a time resolution of 130 ms.

Fig. 6 represents an example of the difference pressures (related to air pressure) as functions of time for the three measuring chambers.

The test vessel contains an $O_2/N_2$ gas mixture of 53/49 kPa. The pressure increases were recorded with an offset at the start of measurement. This offset of about 10 s was chosen uniformly for all experiments, in order to exclude short term interference signals. Such interferences occur due to equilibration of pressure difference inside the measuring chambers, temperature equilibration, and relaxation of pressure sensors.

Because of technical problems during the relatively long conditioning time (some hours), such as instable gas supply, temperature and pressure changes, etc., 10 of the 78 measurements (26 experiments × measurements in three measuring chambers) had to be discarded.

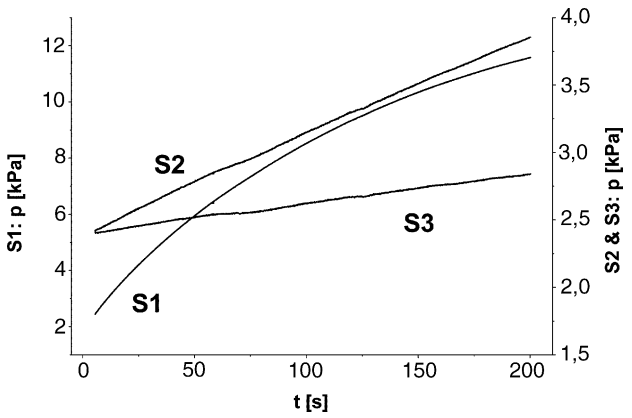


Fig. 6. Time dependence of the pressures $p^i$ during the measurement step. Example for a $O_2/N_2$ gas mixture of 53/49 kPa.

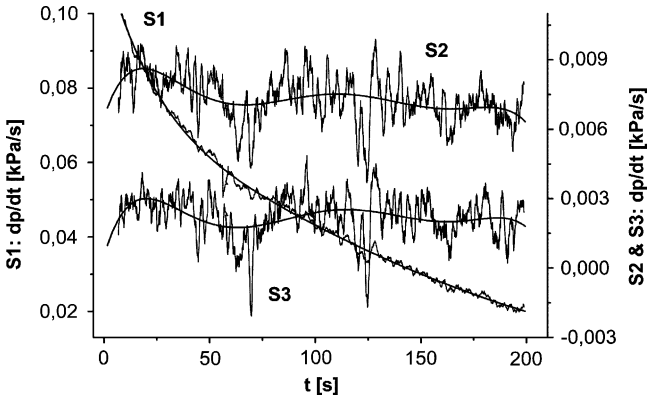


Fig. 7. Time dependence of the pressure change $dp^i/dt$ during the measurement step (example from Fig. 6).

### 3.4. Calculation method

Fig. 7 shows the pressure derivative $dp^i/dt$ as function of time for the experiment presented in Fig. 6. Consider first the measuring chamber S1, the $dp^i/dt$-*curve* drops significantly and in a non-linear way and shows only slight oscillations. This behaviour is consistent with our proposed model: Using Eq. (18) one anticipates a monotonous decrease of $dp^i/dt$ *with time*.

Compared to this the mean curves for the measuring chambers S2 and S3 remain nearly constant over the considered time period. The second difference to the S1-signal run are the strong oscillations. Note that the S2- and S3-curves show the same (synchronous) signal variation (interference signal), which is superposed with the signal of interest.

Both cases provide suitable limit cases for proving the efficiency of the measuring technique.

In order to evaluate the different signal runs over time, the key parameter $a_1$, which determines for $t \to 0$ the pressure change, has to be calculated (see Eq.(17)).

For the S1-chamber (silicone membrane) the signal was approximated by a polynomial of degree 7, whereas the signals for the S2 (Tygon)- and S3 (C Flex)-chambers were approximated by a second order approach.

In order to check the suitability for automated evaluation of the measurements this algorithm was applied uniformly to all data records.

Two calculation methods were used:

#### 3.4.1. Method 1

Applying Dalton's law 1 gas component can be determined by the $n-1$ gas components and the measurement of the total gas pressure. In our two-component system, we have only to determine $a_1$ for oxygen. The corresponding formula is

$$p^{\mathrm{a}}_{\mathrm{O}_2} = \frac{1}{f^k_{\mathrm{O}_2,\mathrm{N}_2} - 1}\left\{ p^k_0 - p^{\mathrm{a}} + \frac{a^k_1}{g^k P^k_{\mathrm{N}_2}} \right\}, \tag{26}$$

where we have substituted $\mathrm{pN}_2$ in Eq. (22) by $p^{\mathrm{a}} - p_{\mathrm{O}_2}$ according to Eq. (24). In this case the balance criterion Eq. (23) is a priori satisfied.

#### 3.4.2. Method 2

The more challenging method consists in an independent evaluation of each gas component from the linear coefficients $a_1$ by solving the system of linear equations (Eq. (22)). If the total gas pressure is known, one can prove, whether Dalton's law is satisfied (balance criterion Eq. (23)). The use of two membrane tubes for determining a two-component gas is the equivalent to the "*n* gas components–*n* membranes"-sensor.

Method 1 was applied both for the parameter identification of the membranes and for partial pressure measurement. Due to its comparably greater number of parameters, Method 2 was used only for the partial pressure estimation.

### 3.5. Evaluation

One half of the experiments was taken for the calibration of the gas sensor (dataset 1) and the other half for the gas analysis (dataset 2), i.e. for the determination of the partial pressures.

#### 3.5.1. Calibration

During calibration, $P_{\mathrm{N}_2}$ and $f_{\mathrm{O}_2/\mathrm{N}_2}$ were fitted by means of the inverse solution of Eq. (26) using the dataset 1 consisting of 12 records for the $a_1$-determination and the known partial pressures $p_{\mathrm{O}_2}$ and $p_{\mathrm{N}_2}$. Fig. 8 shows

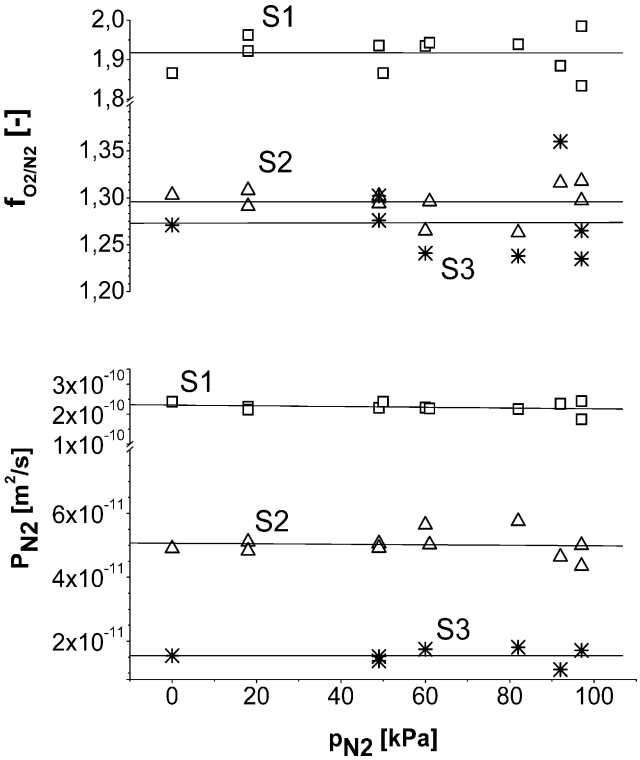


Fig. 8. Membrane calibration. (Top) permselectivity, (bottom) permeability.

Table 2
Membrane calibration: parameter set of the best fit

| Membrane | $P_{N_2} \times 10^{11}$ ($m^2\,s^{-1}$) | $dP_{N_2}/dp_{N_2} \times 10^{11}$ ($m^2\,s^{-1}\,kPa^{-1}$) | $f_{O_2/N_2}$ | $df_{O_2/N_2}/p_{N_2} \times 10^4$ ($kPa^{-1}$) |
|---|---|---|---|---|
| S1 | $23 \pm 1$ | $-0.01 \pm 0.01$ | $1.92 \pm 0.03$ | $-0.03 \pm 4$ |
| S2 | $5.1 \pm 2$ | $-0.0008 \pm 0.004$ | $1.30 \pm 0.01$ | $-0.003 \pm 2$ |
| S3 | $1.5 \pm 0.2$ | $0.00003 \pm 0.003$ | $1.27 \pm 0.04$ | $0.07 \pm 5$ |

the best fits (linear regressions) over the corresponding permeabilities and permselectivities. Table 2 contains the best fit parameters obtained for the gas sensor.

The main reason for the increasing spreading towards lower $O_2$ partial pressures is the varying air pressure (see below).

The permselectivities of the used membranes are relatively low. This restricts the accuracy as shown below. However, membranes with considerably higher permselectivity values are known from literature. For example, a $O_2/N_2$ permselectivity of 28 has been found for poly-aniline membranes over two hours [11], and $O_2/N_2$ permselectivity values of more than 25 were forecast as early as in 1992 [12].

According to the theoretical assumptions both the permeation coefficients $P_{N_2}$ and the permselectivity coefficients $f_{O_2/N_2}$ are constant in the measurement range. Thus, only

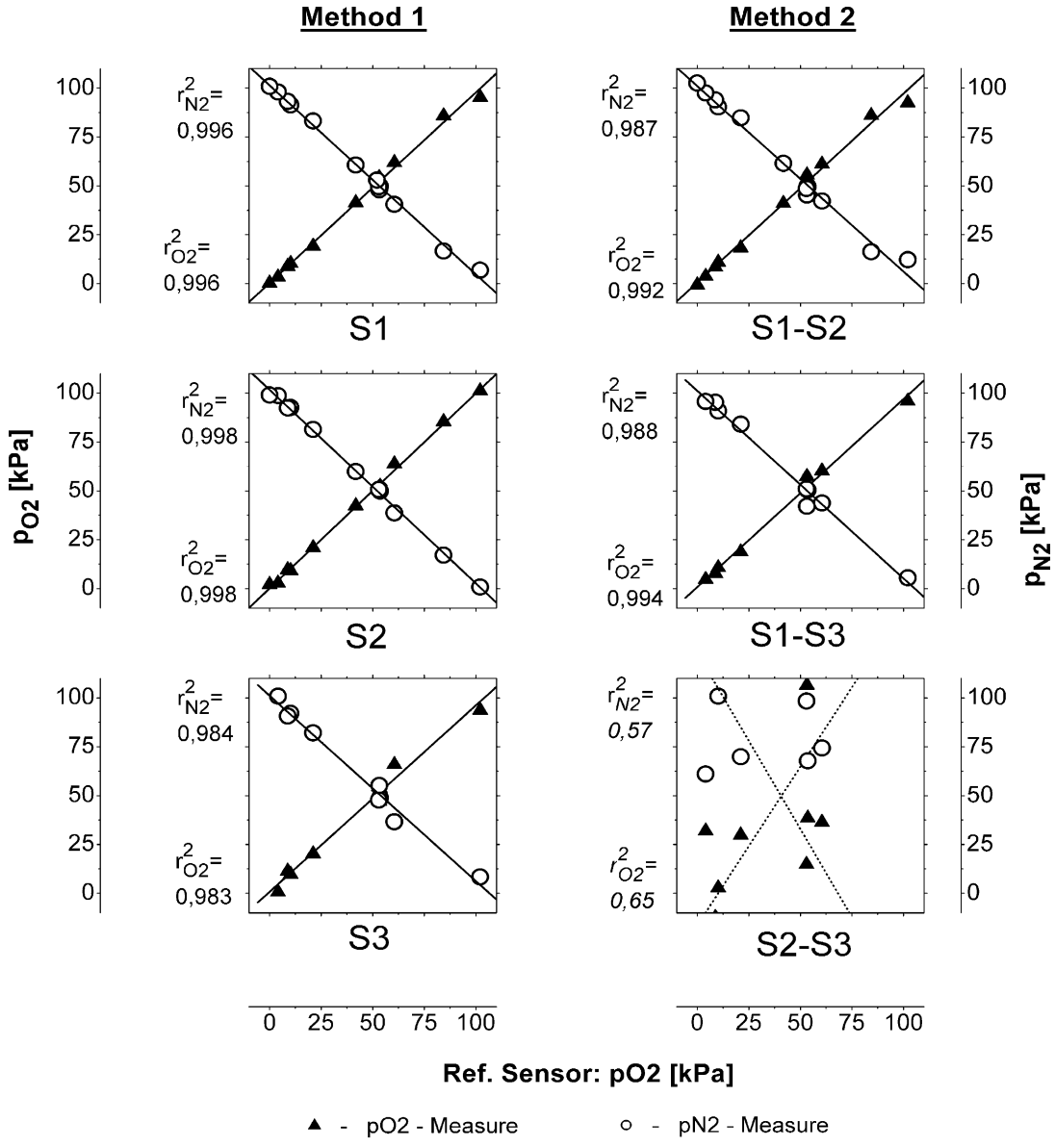


Fig. 9. Measuring comparison: membrane-based gas sensor—reference sensor ($r^2$—squared Pearson's correlation coefficient, lines—linear regressions).

the partial pressure-independent absolute terms for both coefficients (Table 2, columns 2 and 4) were inserted into the equations for the following measurement comparison.

### 3.5.2. Partial pressure measurement

The partial pressure analyses for validating the measurement technique, which were carried out by means of the calibrated gas sensor, are represented in Fig. 9.

Except for the gas sensor established by measuring chambers S2–S3 according to Method 2, all sensor variants show an unexpected high sensitivity to the concentration of both gases. *Note*: The $N_2$ partial pressure in the test vessel is really determined from pressure changes in the measuring chambers in Method 2 and without any additional information!

According to Method 2, the permselectivity is replaced by the difference between the permselectivity of the different membranes in the denominator of the equations to be solved. Therefore this method is more sensitive to measuring errors. Table 2 yields for the membrane systems S1–S2: $\Delta f_{O_2/N_2} \approx 0.62$, S1–S3: $\Delta f_{O_2/N_2} \approx 0.65$, and for S2–S3: $\Delta f_{O_2/N_2} \approx 0.03$. Within the scope of calibration, permselectivity values for the membrane system S2–S3 differ only slightly. Lacking sensitivity of the sensor formed by S2–S3 proves that pressure measurement errors are predominant, while sensor variants using S1 provide usable results.

The main reason for the error is the synchronous signal oscillation (noise) shown in Fig. 7, which occurs in measuring chamber 1, too. Due to its stronger signal to noise ratio, the interference exerts here only a minor effect on the latter. The reason for the signal oscillation were fluctuations of air pressure (mainly due to the air-conditioning system of the building), which served as reference pressure for the sensors used.

### 3.5.3. Error discussion

Due to the low number of measurement points and the analysis range covering three orders of magnitudes, the measurement error was calculated in terms of the mean relative absolute-error of the analyses:

$$\frac{\mathrm{d}p^{\mathrm{a}}_{ji}}{p^{\mathrm{a}}_{ji}} \approx \frac{\left|p^{\mathrm{a}}_{ji} - p^{\mathrm{ref}}_{ji}\right|}{p^{\mathrm{ref}}_{ji}} \tag{27a}$$

$$\delta p^{\mathrm{a}}_{j} = \left(\frac{\overline{dp^{\mathrm{a}}_{j}}}{p^{\mathrm{a}}_{j}}\right) \approx \frac{1}{n}\sum_{i=1}^{n}\frac{\mathrm{d}p^{\mathrm{a}}_{ji}}{p^{\mathrm{a}}_{ji}} \tag{27b}$$

where $p^{\mathrm{a}}_{ji}$ [Pa] is certain partial pressure of gas j in the test vessel during measurement i, $p^{\mathrm{ref}}_{ji}$ [Pa] is corresponding reference measurement value.

The relative absolute-error according to Eq. (27a) exhibits a potentially present error dependence on scale, because of the independence of the expected measurement value (estimated by reference measuring method) and, because of linearity in Eq. (27a), does not lead to a disproportionate evaluation of error differences.

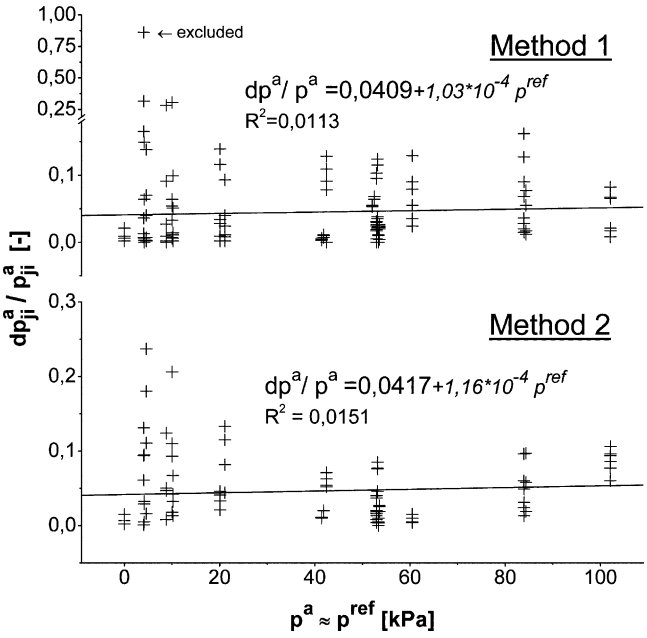


Fig. 10. Method-dependent error distribution of partial pressure measurements. The insensitive sensor S2–S3 (Method 2) is excluded. Remark: all error calculations include the error of the reference of about 1% (see footnote 4) therefore holds $p^{\mathrm{a}} \approx p^{\mathrm{ref}}$.

Fig. 10 shows the error plot of the single measurements according to Eq. (27a) as an $O_2$ partial pressure function. The non-sensitive measuring chamber system S2–S3 (Method 2) shown in Fig. 9 was excluded. The method-dependent means of the overall error were approximated through regression lines. Both the low correlation coefficients and especially the low linear regression coefficients indicate error independence of scale for the range examined.

Table 3
Mean error (a) for sensor calibration and (b) for gas measurement in % of the measuring value

| (a) Sensor calibration | | Gas component | | |
|---|---|---|---|---|
| | Sensor | $O_2$ | $N_2$ | Mean |
| Method 1; dataset 1 | S1 | 3.7 | 2.4 | 3.1 |
| | S2 | 4.3 | 3.7 | 4.0 |
| | S3 | 10.9 | 3.5 | 7.2 |
| (b) Measurement comparison | | Gas component | | |
| | Sensor | $O_2$ | $N_2$ | mean |
| Method 1; dataset 2 | S1 | 4.1 | 2.2 | 3.1 |
| | S2 | 6.2 | 2.6 | 4.4 |
| | S3 | 19.4 | 4.6 | 12.0 |
| Method 2; dataset 1 | S1–S2 | 6.4 | 2.8 | 4.6 |
| | S1–S3 | 8.0 | 3.0 | 5.5 |
| | S2–S3 | 106.0 | 33.8 | 69.9 |
| Method 2; dataset 2 | S1–S2 | 5.0 | 2.8 | 3.9 |
| | S1–S3 | 7.5 | 4.2 | 5.9 |
| | S2–S3 | 171.2 | 56.2 | 113.7 |

This allows the statement of an analysis error related to the measurement value. The analysis error calculated according to Eq. (27b) is indicated for individual sensors in per cent, i.e. multiplied by 100%, in Table 3. The "mean" stated correspond to the mean errors of gas analyses.

Besides the errors obtained for S1 and S2, which are relatively low, Table 3 shows the correlation of errors from calibration and measurement and that of error and permeability (calibration: see Fig. 8). Moreover, the relatively constant error in Fig. 10 suggests that the examination range limited by the experimental set-up does not reproduce the potential measurement range of the sensor.

## 4. Results

In this study, a methodological basis of a new gas-measuring principle was given and was demonstrated for a two-component-gas phase: nitrogen and oxygen. Therefore, a relatively low error range for gas measurement is shown in the order of 5% of the measurement value. Limitations of the considered measurement range are caused by the experimental equipment.

The relatively simple and robust gas measurement method acts completely on the basis of physical principles. Therefore, the method can be used theoretically in multi-purpose applications and it is able to substitute other cost-intensive measuring techniques.

The sensor developed is suited for two types of measurement/monitoring tasks: on the one hand side large sensitive membranes (tubes, networks) can be installed into/onto objects to be observed in order to provide a representative measure. On the other hand a miniaturization of the sensor (micro system) seems to be possible due to utilization of the intensive state variable: pressure.

The general validity of the polynomial fit approach Eq. (16) for estimation of $a_1$ according to Eq. (17) was shown by simultaneous applying of polynomials of the degree 2 for S2, S3 and a polynomial of the degree 7 for S1, respectively.

For a given geometry Eq. (21) scales the linear coefficient $a_1$ by the permeability $P_s$ of the purging gas. With respect to the measurement conditions the purging gas acts therefore as internal standard.

Eq. (21) show further: the lower the permeability of the purging gas and the higher the permselectivities the higher is the resolution and the lower the measurement error. These sensor properties are supported by the membranes available and by the expected trend of development. A negative logarithmic correlation between permeability and permselectivity (so-called trade-off relation) was shown to exist generally by theoretical investigations [13]. The result was experimentally confirmed using 300 glassy polymers and six gases (He, $H_2$, $O_2$, $N_2$, $CO_2$, $CH_4$).

In addition to the improvement of accuracy a low permeability range results in low influences of the sensor on the fluid to be studied. Beneath the negligible interaction between sensor and measuring object one expects a strong independence of the sensor from fluid movements along the outer sensor surface.

## 5. Conclusions and further works

The general applicability of the method, its resolution and detection limits are coupled onto the membranes available. Further studies have to been carried out, in order to adapt appropriate membrane sets for the measurement of different multiple-gas systems.

Parameters and boundary conditions of measurements (time window, offset, fit functions, etc.) and the elements of the measuring chambers were selected empirically in this study. Fundamental investigations are necessary to optimize the measurement inclusive the application of the test criterion according to Eq. (23), and also temperature effects have to be taken into account.

A suitable air pressure-independent reference system for pressure measurement needs to be implemented. The permeabilities of the membranes used in the present study differ in one order of magnitude but having the same thickness. From Eq. (25) one realized both (a) the conditioning time differ in the reciprocal order of magnitude and, also the time of reference. In order to form a uniform time of reference the ratios of membrane thickness squared to permeability are to be leveled out for further applications. In addition the membrane thicknesses are to be reduced generally for realizing shorter conditioning periods of time.

## Acknowledgements

Prof. Ludwig Luckner and coworkers, and Dr. Kamusewitz deserve our thanks for helpful discussions. Sebastian Ebert supported us in software development, Carola Bönisch in the preparation of tests. We thank the UFZ Centre for Environmental Research Leipzig–Halle for financial and technical support of our work.

## Appendix A

According to Eq. (11) and taking into account Eq. (13b) the pressure change inside the tube due to the component $k$ can be described through the inhomogeneous ordinary differential equation:

$$\frac{\mathrm{d}p_k^i}{\mathrm{d}t} = \kappa_k(p_k^{\mathrm{a}} - p_k^i) \tag{A.1}$$

with

$$\kappa_k = gP_k. \tag{A.2}$$

For very thin membranes with negligible curvature the concentration gradient becomes linear within the membrane and

Eq. (A.1) holds exactly. Integration yields

$$p_k^i = \text{const}(t)\exp(-\kappa_k t) \tag{A.3}$$

Inserting Eq. (A.3) into Eq. (A.1) leads to:

$$\begin{aligned}\text{const}(t) &= \kappa_k p_k^{\text{a}} \cdot \int \exp(\kappa_k t)\mathrm{d}t \\ &= p_k^{\text{a}} \exp(\kappa_k t) + \text{const}(t=0).\end{aligned} \tag{A.4}$$

Finally, the unknown integration constant const $(t = 0)$ can be determined by inserted Eq. (A.4) into Eq. (A.3) taking into account the initial condition

$$p_k^i(t=0) = \left. p_k^i \right|_{t=0}, \tag{A.5}$$

and one obtains Eq. (18).

## References


[1] W. Bedingham, J.R. Dufresne, D.F. Wirt, Catheter and probe-catheter assembly, US Patent 5 333 609 (August 1992).

[2] J. Kesson, The diffusion of gases through a silicone rubber membrane, and its application to an in-line carbonation meter, Tech. Q. Master Brew. Assoc. Am. 21 (3) (1984) 143–146.

[3] M. Straková, E. Matisová, P. Šimon, J. Annus, J.M. Lisý, Silicone membrane measuring system with $SnO_2$ gas sensor for on-line monitoring of volatile organic compounds in water, Sens. Actuators B 52 (1998) 274–282.

[4] F. Zee, J.W. Judy, Micromachined polymer-based chemical gas sensor array, Sens. Actuators B 72 (2001) 120–128.

[5] H. Nanto, N. Dougami, T. Mukai, M. Habara, E. Kusano, A. Kinbara, T. Ogawa, T. Oyabu, A smart gas sensor using polymer-film-coated quartz resonator microbalance, Sens. Actuators B 66 (2000) 16–18.

[6] J. Watson, R. Tamadoni, N. McMurray, G.S.V. Coles, Gas monitoring instrument utilising fibre optic, piezoelectric and gas-sensitive polymer techniques, Sens. Actuators B 34 (1996) 323–327.

[7] R.F. Weiss, Permeable membrane gas saturometer, US Patent 3 871 228 (March 1975).

[8] J. Kesson, Method of and apparatus for monitoring concentration of gas in a liquid, US Patent 4 550 590 (November 1985).

[9] J.M. Hale, E. Weber, Method and apparatus for monitoring gas concentration in a fluid, European Patent Application 0 429 397 A2 (May 1991).

[10] D. Lazik, H. Geistlinger, Method for the measuring the concentration or the partial pressure of gases, especially oxygen, in fluids and a corresponding gas sensor, European Patent 1 157 265 (August 2003).

[11] Y.M. Lee, S.Y. Ha, Y.K. Lee, D.H. Suh, S.Y. Hong, Gas separation through conductive polymer membranes. 2. Polyaniline membranes with high oxygen selectivity, Ind. Eng. Chem. Res. 38 (1999) 5.

[12] H. Nishide, E. Tsuchida, in: N. Toshima (Ed.), Polymers for Gas Separation, VCH Publishers, New York, 1992, pp. 183–220 (Chapter 6).

[13] A.Yu. Alentiev, Yu.P. Yampolskii, Free volume model and tradeoff relations of gas permeability and selectivity in glassy polymers, J. Membr. Sci. 165 (2000) 201–216.


## Biographies

*Detlef Lazik* (Dr. rer. nat.), geophysicist & hydrogeologist (German, born in 1960); high school degree in 1979; 1982–1986 studies of Geophysics, 1986–1989 research study in environmental physics, Technical University Mining Academy Freiberg, 1989–1990 postgraduate study of Hydrogeology, Technical University of Dresden. Geophysicist Diploma in 1989, PhD 1990, hydrogeology degree "Groundwater" 1992. 1990–1992 postdoctoral research fellow at the GSF Neuherberg. Since 1992 head of the Lab for Experimental Simulation, Department of Hydrogeology, UFZ—Centre for Environmental Research.

*Helmut Geistlinger* (Dr. rer. nat. Dr. Ing.-habil.) theoretical physicist and modeller (born 1955). 1975–1980 studies of Physics, University of Leipzig, Diploma in 1980; 1980–1983 PhD student and from 1984–1986 postdoctoral fellow at the Department of Theoretical Physics at the University of Leipzig. 1994 Habilitation on oxygen-micro-sensors at the Technical University of Ilmenau. Research stays at the Centre of Chemical Sensors, University of Pennsylvania 1994 and 1995. Previous appointments: 1987–1991 Group Leader of the Chemical Sensor Group at the Technical University Leipzig, 1991–1997; assistant of scientific director/UFZ—Centre for Environmental Research, Current position: Modeling Group Leader, Department of Hydrogeology.